PHYSICS

A single-atom 3D sub-attonewton force sensor

Valdis Blūms,[1] Marcin Piotrowski,[1,2] Mahmood I. Hussain,[1] Benjamin G. Norton,[1] Steven C. Connell,[1,2] Stephen Gensemer,[1,2] Mirko Lobino,[1,3] Erik W. Streed[1,4]*

Forces drive all physical interactions. High-sensitivity measurement of the effect of forces enables the quantitative investigation of physical phenomena. Laser-cooled trapped atomic ions are a well-controlled quantum system whose low mass, strong Coulomb interaction, and readily detectable fluorescence signal make them a favorable platform for precision metrology. We demonstrate a three-dimensional sub-attonewton sensitivity force sensor based on a super-resolution imaging of a single trapped ion. The force is detected by measuring the ion's displacement in three dimensions with nanometer precision. Observed sensitivities were 372 ± 9, 347 ± 18, and 808 ± 51 zN/$\sqrt{\text{Hz}}$, corresponding to 24×, 87×, and 21× above the quantum limit. We verified this technique by measuring a 95-zN light pressure force, an important systematic effect in optically based sensors.

INTRODUCTION

Since the advent of Newton's mechanics, force has been at the forefront of our quantitative description of physical interactions. Ultrasensitive force measurements are an important tool for investigating the fundamental physics of magnetic (*1*, *2*), atomic (*3*), quantum (*4*, *5*), and surface (*6*–*8*) phenomena. Force measurement is also an implicitly important quantity in the systematics of precision measurement of other physical quantities such as the effect of gravity on time in general relativity (*9*). The development of high-resolution imaging of laser-cooled trapped ions (*10*–*12*) opened the possibility for the realization of an ion-based sensor that could resolve an external force in all three directions using a single atomic ion. In a harmonic potential, Hooke's law $F_i = k_i \Delta x_i$ allows us to convert displacement measurements Δx_i into a force measurement F_i through the associated spring constants k_i. Forces parallel to the image plane are detected by measuring the displacement of the ion's centroid, whereas forces applied orthogonal to that plane in the focusing direction, parallel to the optical axis of the imaging apparatus, are measured from a change in the width of a slightly defocused ion image. Although the resolution of a fluorescence image is limited by the wavelength of light, the exact centroid location and width can be determined to a much greater precision through super-resolution imaging techniques (*13*, *14*). Doppler velocimetry–based force sensing in Penning (*15*, *16*) and Paul (*17*) traps has demonstrated sensitivities down to 28 yN/ion/$\sqrt{\text{Hz}}$; however, this is limited to one dimension and a narrow frequency band around a driven oscillation. Force measurement through imaging is a broadband rather than a narrowband sensing technique, with no fundamental lower frequency limit, and upper limit set by the speed and efficiency of the detection apparatus and the ion's scattering rate.

RESULTS

Experimental setup, ion image size, and ion localization

Our ion trapping apparatus (*10*, *18*–*20*) is shown in Fig. 1. A single $^{174}Yb^+$ ion is confined in a Paul trap formed near the electric field zero of a three-dimensional (3D) quadrupole created by radio frequency (RF) excitation of two tungsten needles. The ion is loaded by isotope selective photoionization and laser-cooled to near the Doppler limit of 0.5 mK with λ = 369.5 nm radiation on the $^2S_{1/2}$ to $^2P_{1/2}$ transition. The resulting fluorescence at λ = 369.5 nm is collected using a 0.64 numerical aperture (NA) binary phase Fresnel lens with near wavelength resolution (*10*) and imaged onto an Andor iXon 897 cooled electron-multiplying charge-coupled device (EMCCD) camera with a total magnification M = 395.9 ± 0.6.

A typical in-focus image of our trapped ion is shown in Fig. 2 with full width at half maximum (FWHM) diameters of 378 ± 1 and 393 ± 1 nm in x and y. With a typical 20-s exposure time and accounting for systematic drifts, we are able to determine the ion's centroid position with a precision of 2.8 and 10 nm in the x and y directions, respectively, by fitting to a 2D Gaussian function. Reanalysis of a previous reference fluorescence image in Fig. 2D in the study by Streed *et al.* (*20*), taken with the same apparatus and an exposure time of 60 s, gave similar fitting results. Displacements of the ion parallel to the xy imaging plane are thus directly measured from the translation in the centroid of the ion's image.

When in focus, the ion image is not sensitive to motion along z to first order, so to sense along this axis, we deliberately image the ion slightly out of focus. A displacement of the ion parallel to the optical axis of the system z thus leads to a change in the spot size. We calibrated the image width to z displacement in our system by translating the camera along the optical axis with the ion in a fixed position within the trap. With known magnification parameters and camera translations, we were then able to determine the ion shift along z from changes in the waist of its image with an accuracy of 24 nm, 1% of the 2.4 ± 0.1–μm depth of focus (*10*).

Force sensing calibration

To characterize the system's ability to measure small forces, we performed a series of measurements of ion displacements under the influence of different applied external electrostatic fields. Inside the vacuum chamber, there are three additional electrodes of electropolished stainless steel 2 mm away from the ion for compensating out residual electrostatic fields. We applied an additional voltage on one of these electrodes to deliberately impose a small external electrostatic field to the ion, which did not measurably shift the trapping frequencies. The ion's displacement was measured by taking images with and without the applied voltage to measure the effect of the external force while also capturing the background drift of the ion position. Care was taken to ensure high stability and low drift in the applied voltage source.

[1]Centre for Quantum Dynamics, Griffith University, Brisbane, Queensland 4111, Australia. [2]Commonwealth Scientific and Industrial Research Organisation Manufacturing, Pullenvale, Queensland 4069, Australia. [3]Queensland Micro and Nanotechnology Centre, Griffith University, Brisbane, Queensland 4111, Australia. [4]Institute for Glycomics, Griffith University, Gold Coast, Queensland 4222, Australia. *Corresponding author. Email: e.streed@griffith.edu.au

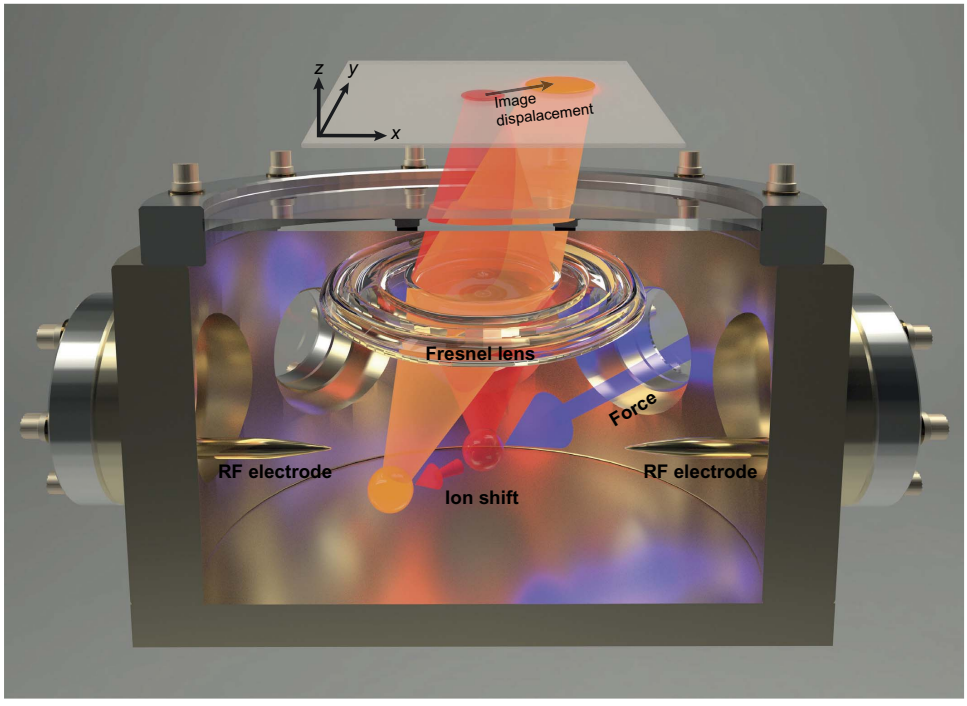

Fig. 1. Experimental configuration. An externally applied force (purple arrow) displaces a trapped $^{174}Yb^{+}$ ion. The image formed by the phase Fresnel lens is shifted in two dimensions. Displacement along the focal axis alters the image spot size. For clarity, illustrated trap dimensions are not to scale. RF electrode needle spacing, 300 μm; lens focal length, 3 mm.

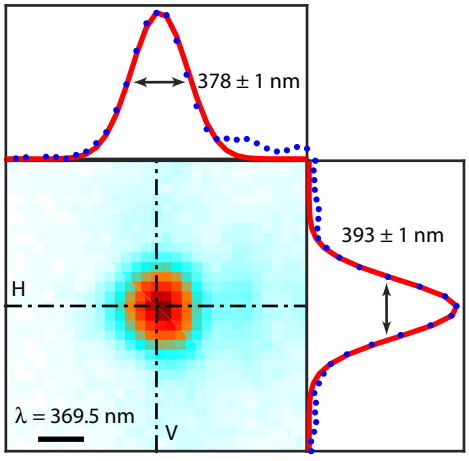

Fig. 2. Ion image. Wavelength-scale ion image with Gaussian fitting and FWHM sizes for the horizontal (H) and vertical (V) slices.

We determine the spring constants $k_i = m\omega_i^2$ of our trap by measuring the secular confinement frequencies ω_i in the three principle axes of our trap through a resonance heating method (*19*). The mass m of $^{174}Yb^{+}$ is presumed to be constant and has been measured (*21*) with an estimated uncertainty of 1.0 ± 10^{-10}. The measured trap frequencies were at 800 ± 1, 829 ± 1, and 1601 ± 1 kHz, corresponding to spring constant values of 7.29 ± 0.02, 7.83 ± 0.02, and 29.22 ± 0.04 zN/nm, respectively. The largest value of the spring constant corresponds to the direction parallel to the trapping needles x, where the confinement is stronger and the trapping frequency is higher. Our 3D quadrupole trap is nearly cylindrically symmetric, and lacking sufficient additional electrodes to break the symmetry in a known direction, we were unable to determine the orientation of the two weaker trapping axes. This introduces a constrained systematic uncertainty of ±7% along those two axes. Although we measured the trap frequencies to ±1 kHz, measurements taken on different days showed a drift of the frequencies of the order of ±15%. This is likely due to variations in the RF electrode needle spacing because they are coupled to nanopositioning stages outside the vacuum system through external mechanical bellows (*18*). For this reason, trap frequencies were collected immediately after the force measurements. Active stabilization of the trap frequencies (*22*) in other ion traps has demonstrated a reduction in the long-term (hours) variations to below the 10^{-5} level. Trap frequency variations could also be reduced below 3×10^{-7} with a more mechanically rigid design combined with further proposed improvements in active and passive stabilization.

Figure 3 (A and B) shows the measured forces on the ion as a function of the applied voltage together with the associated displacement in the x and y directions. Considering the position resolution of our system and the 20-s acquisition time, we measured a sensitivity $S_x = 372 \pm 9$ zN/$\sqrt{\text{Hz}}$ and $S_y = (335, 359) \pm 14$ zN/$\sqrt{\text{Hz}}$, where the range in the value of S_y is due to systematic error associated with the unknown trap axis orientation. The large difference in displacement between Fig. 3A and Fig. 3B is consistent with the difference in spring constant between the stronger confinement in k_x (along the trapping needle axis) and the weaker confinement in k_y (perpendicular to the trapping needle axis) combined with the position of the electrode generating the electrostatic field. Force measurement in the z direction is shown in Fig. 3C together with the corresponding change in position as a function of the external voltage from which we calculated a force sensitivity $S_z = (779, 836) \pm 42$ zN/$\sqrt{\text{Hz}}$. Figure 3 shows the linearity of the

displacement as a function of the applied voltage in all three directions as expected for harmonic potentials with forces up to either 7.5 or 30 aN per axis.

External force test

To independently verify the accuracy of our force sensing technique, we measured the scattering light force from our cooling laser on the ion. Absorption generates a force in the direction of the laser beam $\vec{F} = \gamma\hbar\vec{k}$, proportional to the scattering rate γ and the photon momentum $\hbar\vec{k}$. The spontaneous fluorescence emission is random in direction and does not contribute to a net force when averaged over many scatterings. For an ion near rest, the scattering rate γ is a function of the detuning δ/2π = −14 MHz, the natural linewidth Γ/2π = 19.6 MHz, and the laser saturation $s = P/P_{sat}$ and given by

$$\gamma = \frac{\Gamma}{2}\frac{s}{1 + s + (2\delta/\Gamma)^2} \quad (1)$$

The ion was illuminated with a laser beam along the *y* direction, and the laser power *P* was varied to change the scattering rate and, therefore, the net force. The collected ion fluorescence was split 50/50 between a photomultiplier tube (PMT) and the camera. The inset in Fig. 4 shows the saturation of the PMT counts as a function of the laser power, allowing us to fit for P_{sat} and calibrate the scattering rate. Figure 4 shows the ion displacement as a function of the applied force, together with a linear fit for forces up to 95 zN. From this measurement, we calculated a drifted trap frequency in the *y* axis of 635 ± 25 kHz. The sensitivity of the ion as a force sensor increases by lowering the trapping potential and likewise the associated spring constant and secular frequencies. In our system, the reduction in trap depth is limited by technical noise and likely aggravated by the close proximity (3 mm) of the phase Fresnel lens' dielectric surface (*8*).

Force sensing limitations

Fundamental quantum limits to measuring the average ion position arise from the finite number of photons collected (*13*). For a displacement accuracy of δx_i, we can measure a force with uncertainty $\delta F_i = k_i \delta x_i$, where k_i are the spring constants. In ion traps, the long-term stability of the spring constants can be below 10^{-5} level with an optimized hardware design (*22*), making their uncertainty contribution negligible. Assuming a Gaussian mode for our imaging (*13*) and ignoring technical limitations from pixelization and background noise, for *N* detected photons at wavelength λ with numerical aperture of NA, the transverse uncertainty in the image plane is at best $\delta x_i = \lambda/(\pi \mathrm{NA}\sqrt{N})$ and $\delta z = 2\lambda/(\pi \mathrm{NA}^2\sqrt{N})$ in the focus direction. In real experiments, the effective quantum limits are reduced due to imaging imperfections.

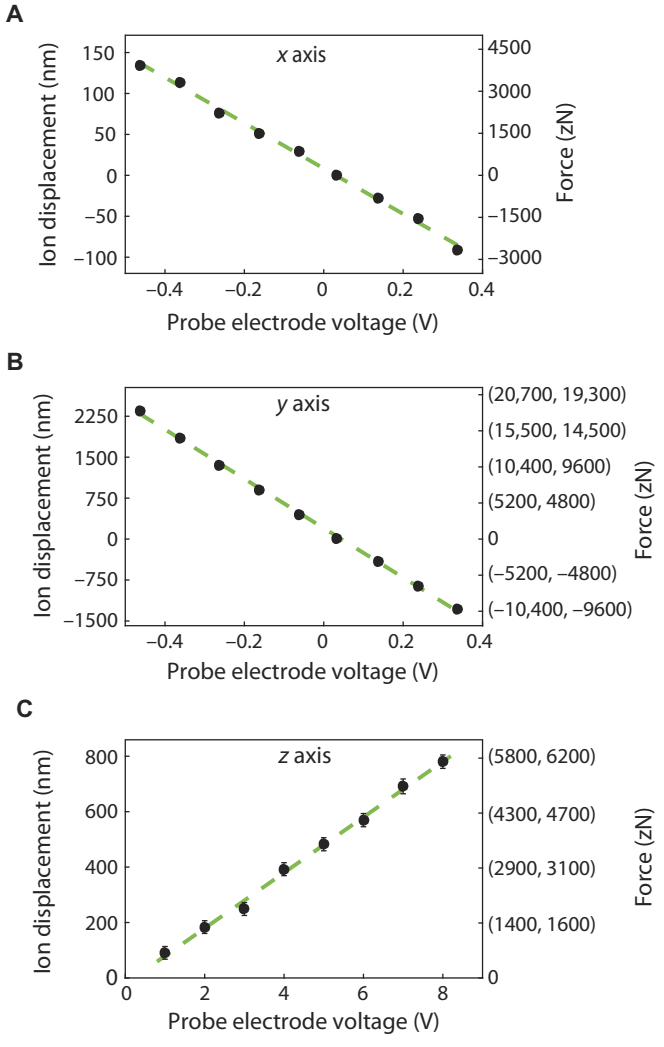

Fig. 3. Electrostatic force detection and ion movement in three axes. *x* and *y* axes refer to camera plane, and *z* axis refers to the optical axis of the imaging system. (**A**) Ion displacement and applied force as a function of the external voltage in the *x* axis. This axis corresponds to the orientation of the trapping needles and has the strongest confinement. (**B**) Same as (A) but for the *y* axis. The use of ranges in the force vertical axis of the plot represents the constrained systematic uncertainty due to unknown orientation of the trap principal axis with respect to our optical system. Error bars in (A) and (B) are smaller than the dots. (**C**) Same as (B) but for the *z* axis.

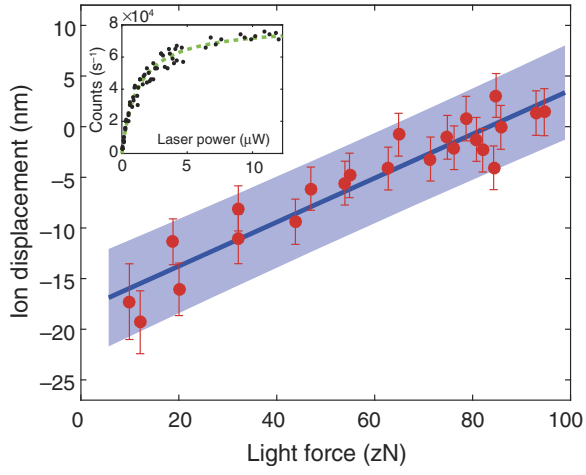

Fig. 4. Light force detection with a single ion. Ion displacement as a function of the light force (red dots) and linear fit to experimental data (blue line). The shaded region shows the 95% confidence level for linear fit to experimental data. Inset: Photons scattered by the ion as a function of the laser power. The green dashed line is the fitted curve from Eq. 1, scaled by the detection efficiency, used for calculating the saturation parameter *s* as a function of the laser power.

Table 1. Error budget. Average errors for the data points in Fig. 3.

	x	*y*	*z*
σ_{fit} (nm)	1.1	1.1	14.3
$\sigma_{DRIFT(fit)}$ (nm)	1.1	1	14.3
$\sigma_{i,DRIFT(interpolation)}$ (nm)	2.4	9.9	12.7

On the basis of these estimates, we are within a factor of (24×, 87×) in the 2D imaging plane (strong, weak confinement directions) and 21× in the focal direction of the quantum limits given our trapping frequencies and imaging performance. The main cause of reduced sensitivity of our apparatus from the quantum limit is the constant drift in ion position, which limits our precision in determining its position. The focusing direction is potentially more susceptible to external noise because random deviations will cause a cumulative increase in the spot width, whereas only the residual unbalanced sum of these deviations will affect the centroid location. Similarly, the strong *x* axis (along the axis of the needles) trap direction will be less vulnerable to wobble in the needle positions than the two weaker (*y* and *z*) confinement axes.

The sensitivity of this technique could be enhanced by matching the trap confinement aspect ratios to the imaging system resolution by symmetrizing the confinement strength in the imaging plane and weakening the confinement along the focal direction. In an RF Paul trap, application of DC curvature potentials redistributes the total spring constant provided by the RF field, allowing alteration of the trap confinement aspect ratios. In our experiment, imaging performance above the diffraction limit accounts for a factor of 2 in the sensitivity in the transverse directions and a factor of 8 in the focus direction. We attribute most of our error to mechanical drift because our system was not specifically engineered for long-term stability at the nanometer scale, although the required stability could be readily achieved with a suitably designed system.

DISCUSSION

The imaging-based trapped single ion force sensor demonstrated here uses nanometer-scale spatial resolution in all three dimensions to obtain sub-attonewton sensitivities of 372 ± 9 stat, 347 ± 12 sys ± 14 stat, and 808 ± 29 sys ± 42 stat zN/$\sqrt{\text{Hz}}$. It has important implications for a number of practical areas of physical investigation, including for use as an in-trap probe of higher-order electric fields from a co-trapped particle, such as the permanent electrical dipole moment of a biomolecule (*23*) or nanoparticle (*24*), or investigation of surface properties (*8*). This type of measurement is similar to the attonewton sensitivity 2D force sensing recently demonstrated with atomic force microscopy (*6*, *7*), but with substantially higher sensitivity and potential for future improvements. The near-field optical interactions with a surface could ultimately limit our scheme at small (<~100 nm) distances, although at present, surface phenomena that drive electrical noise limit working surface-ion distances to tens of micrometers (*25*). This technology can be scaled up to imaging multiple ions trapped and imaged together and used for high sensitivity and high spatial resolution study of a force field distribution.

MATERIALS AND METHODS

Magnification calibration

Image magnification is crucial for linking a change of the ion's image position on the CCD camera to the ion's actual displacement within the trap. To accurately calibrate the magnification of our system, we measured the separation of two trapped ions (*10*) that were aligned parallel to the *x* axis by applying a negative DC voltage to the RF needles. Because of the Coulomb repulsion, if two ions are trapped simultaneously, then their separation is given by

$$l = \left(\frac{e^2}{8\pi\epsilon_0 m\nu^2}\right)^{1/3} = 4.6 \pm 0.005\ \mu\text{m} \quad (2)$$

where *e* is the electron charge, ϵ_0 is the permittivity of free space, *m* is the mass of each $^{174}Yb^+$ ion, and $\nu = 643 \pm 1$ kHz is the secular frequency of the ions along the axis of separation. The distance between ions measured from the camera was 114 ± 0.1 pixels or 1824.5 ± 1.7 μm in the image plane. From these data, we calculated a magnification of $M = 395.9 \pm 0.6$. The magnification obtained from this method was validated by mechanically translating the RF needles 1 μm and verifying that the ion image was displaced by the expected amount.

Data acquisition routine

We developed a special routine of data acquisition to measure absolute change of the ion position under the influence of external forces. The drifts of ion position within the trap are of the order of tens of nanometers per hour. This is a main consequence of the fact that the trap used for this experiment was not designed for nanometer-level stability. To suppress the effects of drift on the force measurements, we chopped the applied force on and off at a rate equal to two times the camera integration time of 20 s and subtracted the changing drift from the force measurements. The drift value at the data point time was calculated by linear interpolation between the two neighboring drift points and used to determine the differential displacement of the ion position, which reflects the actual influence of applied force. Several different interpolation methods were investigated (moving spline, low-order polynomial, averaging two drift points); however, they all output approximately the same results.

Error budget

The main cause of error in our apparatus was the presence of drift, which limits the accuracy of the ion's displacement measurements. Statistical uncertainty of the Gaussian fit of ion image position on the CCD camera σ_{fit} and the statistical uncertainty of the Gaussian fit of positions of two adjacent drift points $\sigma_{DRIFT(fit)}$ are of the order of 1 nm for the *x* and *y* axis and 14.3 nm for the *z* axis. The drift error is limited by the sampling rate of the drift dynamic because of our 20-s integration time and the linear interpolation used to estimate the value of the drift at a specific data point.

We estimated the drift interpolation uncertainty $\sigma_{i,DRIFT(interpolation)}$ by taking the position of a drift point along one axis $x_{i,d}$, calculating its distance from the linear interpolation between the two adjacent points $x_{i-1,d}$ and $x_{i+1,d}$ and dividing it by 2 because the data images are acquired in between drift measurements. The drift interpolation error for each axis measurement is the average of the $\sigma_{i,DRIFT(interpolation)}$ for the individual points. The total uncertainty for the ion displacement measurement σ_{ion}, expressed as error bars on the graphs in Fig. 3, is given by $\sigma^2_{ion} = \sigma^2_{fit} + \sigma^2_{DRIFT(fit)} + \sigma^2_{DRIFT(interpolation)}$, and the values of the error contributions for the three axes are reported in Table 1.

SUPPLEMENTARY MATERIALS

Supplementary material for this article is available at http://advances.sciencemag.org/cgi/content/full/4/3/eaao4453/DC1
section S1. Quantum limit
section S2. Constant mass assumption
section S3. Image spot width limitations
Reference (*26*)

REFERENCES AND NOTES

1. D. Rugar, R. Budakian, H. J. Mamin, B. W. Chui, Single spin detection by magnetic resonance force microscopy. *Nature* **430**, 329–332 (2004).
2. A. C. Bleszynski-Jayich, W. E. Shanks, B. Peaudecerf, E. Ginossar, F. von Oppen, L. Glazman, J. G. E. Harris, Persistent currents in normal metal rings. *Science* **326**, 272–275 (2009).
3. D. Gangloff, A. Bylinskii, I. Counts, W. Jhe, V. Vuletić, Velocity tuning of friction with two trapped atoms. *Nat. Phys.* **11**, 915–919 (2015).
4. U. Mohideen, A. Roy, Precision measurement of the Casimir force from 0.1 to 0.9 μm. *Phys. Rev. Lett.* **81**, 4549 (1998).
5. H. B. Chan, V. A. Aksyuk, R. N. Kleiman, D. J. Bishop, F. Capasso, Quantum mechanical actuation of microelectromechanical systems by the Casimir force. *Science* **291**, 1941–1944 (2001).
6. L. M. de Lépinay, B. Pigeau, B. Besga, P. Vincent, P. Poncharal, O. Arcizet, A universal and ultrasensitive vectorial nanomechanical sensor for imaging 2D force fields. *Nat. Nanotechnol.* **12**, 156–162 (2016).
7. N. Rossi, F. R. Braakman, D. Cadeddu, D. Vasyukov, G. Tütüncüoglu, A. Fontcuberta i Morral, M. Poggio, Vectorial scanning force microscopy using a nanowire sensor. *Nat. Nanotechnol.* **12**, 150–155 (2016).
8. M. Harlander, M. Brownnutt, W. Hänsel, R. Blatt, Trapped-ion probing of light-induced charging effects on dielectrics. *New J. Phys.* **12**, 093035 (2010).
9. C. W. Chou, D. B. Hume, J. C. J. Koelemeij, D. J. Wineland, T. Rosenband, Frequency comparison of two high-accuracy Al^+ optical clocks. *Phys. Rev. Lett.* **104**, 070802 (2010).
10. A. Jechow, E. W. Streed, B. G. Norton, M. J. Petrasiunas, D. Kielpinski, Wavelength-scale imaging of trapped ions using a phase Fresnel lens. *Opt. Lett.* **36**, 1371–1373 (2011).
11. R. Maiwald, A. Golla, M. Fischer, M. Bader, S. Heugel, B. Chalopin, M. Sondermann, G. Leuchs, Collecting more than half the fluorescence photons from a single ion. *Phys. Rev. A* **86**, 043431 (2012).
12. J. D. Wong-Campos, K. G. Johnson, B. Neyenhuis, J. Mizrahi, C. Monroe, High-resolution adaptive imaging of a single atom. *Nat. Photonics* **10**, 606–610 (2016).
13. R. E. Thompson, D. R. Larson, W. W. Webb, Precise nanometer localization analysis for individual fluorescent probes. *Biophys. J.* **82**, 2775–2783 (2002).
14. A. Pertsinidis, Y. Zhang, S. Chu, Subnanometre single-molecule localization, registration and distance measurements. *Nature* **466**, 647–651 (2010).
15. M. J. Biercuk, H. Uys, J. W. Britton, A. P. VanDevender, J. J. Bollinger, Ultrasensitive detection of force and displacement using trapped ions. *Nat. Nanotechnol.* **5**, 646–650 (2010).
16. K. A. Gilmore, J. G. Bohnet, B. C. Sawyer, J. W. Britton, J. J. Bollinger, Amplitude sensing below the zero-point fluctuations with a two-dimensional trapped-ion mechanical oscillator. *Phys. Rev. Lett.* **118**, 263602 (2017).
17. R. Shaniv, R. Ozeri, Quantum lock-in force sensing using optical clock Doppler velocimetry. *Nat. Commun.* **8**, 14157 (2017).
18. E. W. Streed, B. G. Norton, A. Jechow, T. J. Weinhold, D. Kielpinski, Imaging of trapped ions with a microfabricated optic for quantum information processing. *Phys. Rev. Lett.* **106**, 010502 (2011).
19. B. G. Norton, E. W. Streed, M. J. Petrasiunas, A. Jechow, D. Kielpinski, Millikelvin spatial thermometry of trapped ions. *New J. Phys.* **13**, 113022 (2011).
20. E. W. Streed, A. Jechow, B. G. Norton, D. Kielpinski, Absorption imaging of a single atom. *Nat. Commun.* **3**, 933 (2012).
21. R. Rana, M. Höcker, E. G. Myers, Atomic masses of strontium and ytterbium. *Phys. Rev. A* **86**, 050502 (2012).
22. K. G. Johnson, J. D. Wong-Campos, A. Restelli, K. A. Landsman, B. Neyenhuis, J. Mizrahi, C. Monroe, Active stabilization of ion trap radiofrequency potentials. *Rev. Sci. Instrum.* **87**, 053110 (2016).
23. D. Trypogeorgos, C. J. Foot, Cotrapping different species in ion traps using multiple radio frequencies. *Phys. Rev. A* **94**, 023609 (2016).
24. A. Kuhlicke, A. W. Schell, J. Zoll, O. Benson, Nitrogen vacancy center fluorescence from a submicron diamond cluster levitated in a linear quadrupole ion trap. *Appl. Phys. Lett.* **105**, 073101 (2014).
25. M. Brownnutt, M. Kumph, P. Rabl, R. Blatt, Ion-trap measurements of electric-field noise near surfaces. *Rev. Mod. Phys.* **87**, 1419 (2015).
26. J. D. Valentine, A. E. Rana, Centroid and full-width at half maximum uncertainties of histogrammed data with an underlying Gaussian distribution-the moments method. *IEEE Trans. Nucl. Sci.* **43**, 2501–2508 (1996).

Acknowledgments

Funding: This work was supported by the Australian Research Council (ARC) under DP130101613 and performed as part of the Australian Commonwealth Scientific and Industrial Research Organisation (CSIRO)/Griffith University collaboration. E.W.S was supported by ARC Future Fellowship FT130100472. V.B. and B.G.N. were supported by the Australian Government Research Training Program Scholarship. M.I.H. was supported by the Griffith International Research Higher Degree scholarship. S.C.C. was supported by a CSIRO Scholarship. M.P. was supported by a CSIRO Office of the Chief Executive Postdoctoral Fellowship. The phase Fresnel lens was fabricated by M. Ferstl at the Heinrich-Hertz-Institut of the Fraunhofer-Institut für Nachrichtentechnik in Germany. **Author contributions:** The experiment was conceived and designed by E.W.S., S.G., and B.G.N. The data were taken by V.B., M.I.H., M.P., B.G.N., and S.C.C. on an experimental apparatus constructed by E.W.S., V.B., and B.G.N. The data were analyzed by V.B., S.G., M.P., and M.L. The manuscript was prepared by V.B., M.P., M.L., and E.W.S with input from the remaining authors. The study was supervised by S.G., E.W.S., and M.L. **Competing interests:** The authors declare that they have no competing interests. **Data and materials availability:** All data needed to evaluate the conclusions in the paper are included in the paper and/or the Supplementary Materials. Additional data related to this paper may be requested from the authors.

Submitted 21 July 2017
Accepted 8 February 2018
Published 23 March 2018
10.1126/sciadv.aao4453

Citation: V. Blūms, M. Piotrowski, M. I. Hussain, B. G. Norton, S. C. Connell, S. Gensemer, M. Lobino, E. W. Streed, A single-atom 3D sub-attonewton force sensor. *Sci. Adv.* **4**, eaao4453 (2018).

ScienceAdvances

A single-atom 3D sub-attonewton force sensor

Valdis Blums, Marcin Piotrowski, Mahmood I. Hussain, Benjamin G. Norton, Steven C. Connell, Stephen Gensemer, Mirko Lobino and Erik W. Streed

Sci Adv **4** (3), eaao4453.
DOI: 10.1126/sciadv.aao4453